nature materials

REVIEW ARTICLE

PUBLISHED ONLINE: 23 AUGUST 2010 | DOI: 10.1038/NMAT2810

The Fano resonance in plasmonic nanostructures and metamaterials

Boris Luk'yanchuk[1], Nikolay I. Zheludev[2], Stefan A. Maier[3], Naomi J. Halas[4], Peter Nordlander[5]*, Harald Giessen[6] and Chong Tow Chong[1,7]

Since its discovery, the asymmetric Fano resonance has been a characteristic feature of interacting quantum systems. The shape of this resonance is distinctively different from that of conventional symmetric resonance curves. Recently, the Fano resonance has been found in plasmonic nanoparticles, photonic crystals, and electromagnetic metamaterials. The steep dispersion of the Fano resonance profile promises applications in sensors, lasing, switching, and nonlinear and slow-light devices.

Galileo Galilei recognized the resonance effect in his study of musical strings as early as 1602. Subsequently it was found that resonances — such as mechanical, acoustic and electromagnetic ones — are a universal characteristic of many types of classical and quantum system. The spectral dependence of these resonances is generally described by the Lorentzian formula, with dynamical variables arising from a simple linear differential equation. "But", as Mandelstam said[1], "it is not trivial that it is trivial", implying that this far-reaching analogy between such disparate phenomena has deep physical origins.

For many years, the Lorentzian formula was regarded as the fundamental lineshape of a resonance. This spectral feature is frequently modified by the presence of several independent resonances of different physical origins, where the lineshape is simply the sum of the intensities of the individual resonances that contribute to it. In other words, interference effects owing to interacting resonances are not present in most typical resonance phenomena.

In 1961, in a quantum mechanical study of the autoionizing states of atoms, Ugo Fano discovered a new type of resonance that now bears his name[2]. In contrast to a Lorentzian resonance, the Fano resonance exhibits a distinctly asymmetric shape with the following functional form:

$$I \propto \frac{(F\gamma + \omega - \omega_0)^2}{(\omega - \omega_0)^2 + \gamma^2}$$

where ω_0 and γ are standard parameters that denote the position and width of the resonance, respectively; F is the so-called Fano parameter, which describes the degree of asymmetry. The microscopic origin of the Fano resonance arises from the constructive and destructive interference of a narrow discrete resonance with a broad spectral line or continuum. Subsequent to its discovery, there have been a great number of studies devoted to Fano resonances in various quantum systems, such as quantum dots, nanowires and tunnel junctions[3–6]. For an interesting perspective on some of Fano's work on spectral lineshapes before the publication of the 1961 paper, we refer the reader to a recent review[3].

The Fano resonance has generally been regarded as a feature entirely specific to quantum systems. However, wavefunction interference phenomena are also ubiquitous in classical optics. The first observation of this asymmetric lineshape in optics is probably Wood's anomaly[7]; however, a clear understanding that this phenomenon is related to interference of excited leaky modes with an incoming radiation took some time to emerge. It has recently been shown that the asymmetric profiles of this effect agree well with the Fano formula[8]. Fano resonances have also been observed in the frustrated total internal reflection spectra of prism-coupled square micropillars[9] and in the interactions of narrow Bragg resonances with broad Mie or Fabry–Pérot bands in photonic crystals[10]. The transmission and reflection properties of photonic-crystal slabs also exhibit Fano resonances[11–19]. Over the past few years the Fano resonance has been observed in a number of nanoscale classical oscillator systems enabled by plasmonic nanostructures[17,20–28], along with metamaterials with plasmonic-nanostructure constituents, including diffraction gratings and hole or particle arrays[29–57]. Fano-type transmission/reflection has been observed in light passing through subwavelength apertures in perforated polaritonic membranes[58], metallic films (extraordinary optical transmission[59,60]), random photonic structures[61], and so on. Here we review the basic mechanism of the Fano resonance in plasmonic materials and metamaterials and provide examples of a number of these systems in which the properties support Fano resonances. We also discuss possible applications enabled by this resonance with its unique lineshape.

The Fano resonance

A Fano resonance can appear in Mie theory for light scattering from a single spherical plasmonic particle. In Mie theory[62,63], the extinction, scattering and absorption cross-sections are given by expressions of the form $\sigma = \pi a^2 Q$, where a is the radius of the particle and Q the corresponding efficiency. The scattering efficiency is defined by:

$$Q_{sca} = \frac{2}{q^2}\sum_{\lambda=1}^{\infty}(2\lambda+1)\left\{|a_\lambda|^2 + |b_\lambda|^2\right\} \quad (1)$$

where a_λ and b_λ are electric and magnetic amplitudes, respectively, which depend on the size parameter $q = \omega a/c$ (c is the speed of light in a vacuum and ω the incident-light frequency and also on

[1]Data Storage Institute, Agency for Science, Technology and Research, DSI Building, 5 Engineering Drive 1, Singapore 117608, Singapore, [2]Optoelectronics Research Centre, University of Southampton, Southampton SO17 1BJ, UK, [3]Physics Department, Imperial College London, South Kensington, London SW7 2AZ, UK, [4]Department of Electrical and Computer Engineering, Rice University, Houston, Texas 77005-1892, USA, [5]Department of Physics and Astronomy, Rice University, Houston, Texas 77005-1892, USA, [6]4th Physics Institute, University of Stuttgart, D-70569 Stuttgart, Germany, [7]Department of Electrical and Computer Engineering, National University of Singapore, Singapore 117576, Singapore. *e-mail: nordland@rice.edu

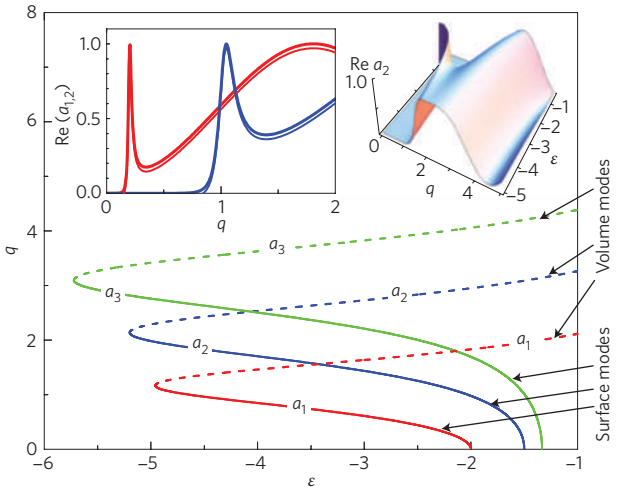

Figure 1 | Trajectories of the three first optical electric resonances a_λ. The lower (solid) branches present the narrow surface plasmon modes and upper (dashed) branches present the broad volume Mie resonances. These two branches converge at certain negative values of ε, for example, at $\varepsilon \approx -5$ and $q \approx 1.2$ for the dipole resonance $\lambda = 1$. Insets show plots of dipole (red) and quadrupole resonances (blue) versus size parameter at $\varepsilon \approx -2.1$ and a three-dimensional plot of quadrupole $\lambda = 2$ electric amplitude on the plane of parameters $\{\varepsilon, q\}$.

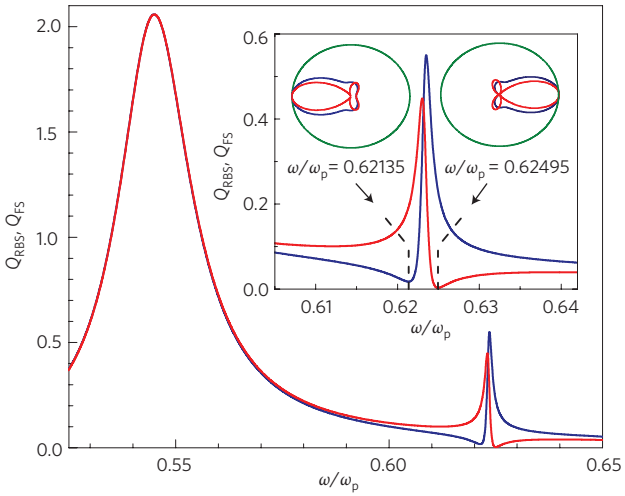

Figure 2 | Mie scattering against a solid metallic sphere. Radar back scattering (RBS; red) and forward scattering (FS; blue) cross-sections versus normalized frequency ω/ω_p. The dielectric permittivity ε is described by the Drude formula, $\gamma/\omega_p = 10^{-3}$ (weak dissipation), where ω_p is the plasma frequency and γ is the collision frequency. Parameter $q = \omega_p a/c = 0.7$. Calculations using equation (3) and the simplified equation (4) differ less than the thickness of the lines. Inset shows polar scattering diagrams in the x–z plane (azimuthal angle $\varphi = 0$ in Mie theory) near the quadrupole resonance of a plasmonic particle. Red lines shows linearly polarized light; blue lines represent non-polarized light.

the dielectric permittivity ε and the magnetic permeability μ. The scattering amplitudes are defined by the Mie formulas:

$$a_\lambda = \frac{\Re_\lambda^{(a)}}{\Re_\lambda^{(a)} + i\Im_\lambda^{(a)}},\ b_\lambda = \frac{\Re_\lambda^{(b)}}{\Re_\lambda^{(b)} + i\Im_\lambda^{(b)}} \qquad (2)$$

The functions $\Re$ and $\Im$ are expressed as combinations of the spherical Bessel and Neumann functions[64]. For a small size parameter $q << 1$ and non-magnetic particle ($\mu = 1$), equation (1) yields the classical formula for Rayleigh scattering:

$$Q_{sca} \approx \frac{8}{3}\left|\frac{\varepsilon - 1}{\varepsilon + 2}\right|^2 q^4$$

This formula holds for positive and negative ε except close to the surface plasmon resonance ($\varepsilon = -2$), where it exhibits a singularity in the absence of intrinsic damping. With increasing size, higher-order eigenmodes (quadrupole ($\lambda = 2$), octupole ($\lambda = 3$) and higher multipoles) become important, giving rise to extra resonances that lead to oscillations in the scattering efficiency (see, for example, Figure 14.13 in ref. 62). For dielectric optical materials with $\varepsilon > 1$, all optical resonances are broad[65], and the requirements for a Fano resonance, that is, the spectral overlap of broad and narrow resonances, cannot be fulfilled. However, with plasmonic materials, the situation is different.

For each angular momentum channel, the plasmon mode can have a very different linewidth. Let us consider for example the dipole resonance. For $-2 < \varepsilon < 0$ and size parameters $q > 1$, this resonance is broad and strongly damped for dissipative materials such as silver and gold. This is because of the large imaginary part of ε near the bulk plasma frequency where these resonances occur for realistic sizes. For $-5 < \varepsilon < -2$ and $q << 1$ the resonance is narrower, and for dissipative materials it is comparatively weakly damped (as they occur at lower frequencies where the imaginary part of epsilon is lower), in particular when $\varepsilon \to -2$. For plasmonic materials, these broad and narrow resonances appear for all eigenmodes and coexist over a range of ε values, as shown in Fig. 1.

For non-dissipative media, the optical resonances are reached at the points where $\Im_\lambda^{(a)} = 0$ (electric resonances) or $\Im_\lambda^{(b)} = 0$ (magnetic resonances). For a small non-magnetic particle $|b_\lambda| << |a_\lambda|$, it follows from equations (1) and (2) that

$$Q_{sca}^{(\lambda)} = \frac{2(2\lambda + 1)}{q^2}$$

where $Q_{sca}^{(\lambda)}$ is the scattering efficiency for the λth mode. The resonance scattering cross-section thus increases with increasing multipolar order λ. This results in an inverse hierarchy of optical resonances[64], in contrast to Rayleigh scattering, where the quadrupole and higher-order resonances are strongly suppressed. This interesting effect of Mie theory for plasmas has been known for a long time[66]. The inset in Fig. 1 clearly shows the coexistence of broad dipole Mie and narrow quadrupole surface plasmon resonances near $q \approx 1$ for a plasmonic material with $\varepsilon = -2.1$.

Fano resonances require an observable that is sensitive to interference. For individual solid structures defined by a single metallic surface, interference does not occur in total scattering or extinction, because the corresponding efficiencies are proportional to the sum of intensities (equation (1)). In multisurface particles such as nanoshells, interferences can be observed in total extinction owing to interactions between the various plasmon modes of the system. For a solid metallic nanosphere, interference can be observed in its differential scattering spectra, such as radar back scattering (RBS)[63] or forward scattering (FS), with the efficiencies:

$$Q_{RBS} = \frac{1}{q^2}\left|\sum_{\lambda=1}^{\infty}(2\lambda + 1)(-1)^\lambda\left[a_\lambda - b_\lambda\right]\right|^2, \qquad (3)$$

$$Q_{FS} = \frac{1}{q^2}\left|\sum_{\lambda=1}^{\infty}(2\lambda + 1)\left[a_\lambda + b_\lambda\right]\right|^2$$

For a small plasmonic particle, the magnetic amplitude is negligible, that is, $b_\lambda << a_\lambda$. Thus, the lowest-energy interference occurs for the dipole ($\lambda = 1$) and quadrupole ($\lambda = 2$) amplitudes

$$Q_{RBS} = \frac{1}{q^2}\left|a_1 - \frac{5}{3}a_2\right|^2, \qquad (4)$$

$$Q_{FS} = \frac{1}{q^2}\left|a_1 + \frac{5}{3}a_2\right|^2$$

In Fig. 2 we show Q_{RBS} and Q_{FS} calculated using equations (1) and (4). The two features appearing in the spectra are the symmetric dipole resonance and the asymmetric quadrupole Fano resonance. The Fano resonance becomes more pronounced for a smaller size parameter and smaller dissipation.

The interaction between the dipolar Mie and quadrupole resonances that give rise to the Fano resonance is a result of radiative coupling[64]. Interference of the incident and re-emitted light generates a complex near-field pattern and may give rise to either strong enhancement (constructive interference) or strong suppression (destructive interference) of the electromagnetic field. This is analogous to the Fano resonances of a quantum particle scattered by a potential with quasidiscrete levels[20,21]. We should emphasize that the coupling of the resonances results from radiative modes produced by localized surface plasmons. This radiation can be seen in the energy flow (Poynting vector)[65,67]. The energy flow near the surface dipole resonance resembles helicoidally shaped vortices (see Fig. 6 in ref. 65). The energy flow near the quadrupole resonance is even more complex, exhibiting singular points and optical vortices (see Fig. 5 in ref. 65).

As can be expected for a strongly dispersive phenomenon such as a Fano resonance, the spatial distribution of scattered light will also be strongly frequency dependent[68]. This is particularly the case for weakly dissipative systems, such as many plasmonic materials. In the inset of Fig. 2 we show scattering diagrams for frequencies near the Fano resonance. Here we see a dramatic variation from forward to backward scattering with only a small change in frequency of the incident light. This unique property may be exploitable in applications such as sensing or optical switching. Similarly, a pair of interacting plasmonic particles can serve as a unidirectional, ultracompact optical nanoantenna[54].

Higher multipolar surface modes can also interfere with the broad dipole mode and generate higher-order Fano resonances when the system size is increased. In Fig. 3a we show the appearance of an octupolar Fano resonance resulting from these higher-order interactions. Experimentally observed higher-order Fano resonances in plasmonic systems are discussed below.

Significant Fano resonances can also occur for materials with negative permeability ($\mu < 0$) and positive dielectric permittivity ($\varepsilon > 0$). Here the lowest-energy magnetic Fano resonance results from interference of the dipole b_1 and quadrupole b_2 magnetic amplitudes, as shown in Fig. 3b.

Even more pronounced Fano resonances may be seen within a material with negative refractive index, where both ε and μ are negative[49]. This is illustrated in Fig. 3c,d, where a large asymmetry of radar back scattering and forward scattering efficiencies in the vicinity of electric and magnetic quadrupole resonances is apparent.

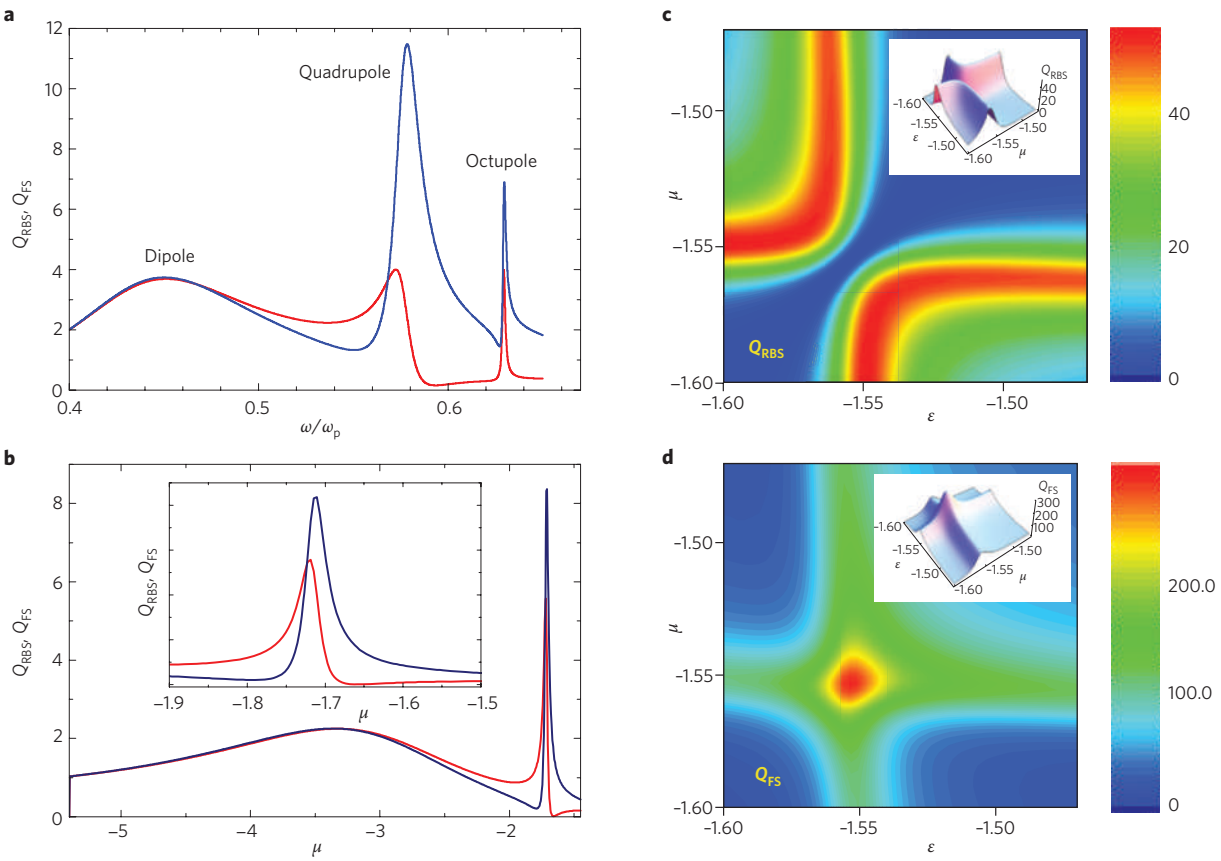

Figure 3 | Higher-order multipolar Fano resonances in Mie scattering against a solid metallic sphere. a, Radar back scattering (red) and forward scattering (blue) cross-sections calculated using equation (3) versus normalized frequency ω/ω_p. The dielectric permittivity ε is described by the Drude formula, $\gamma/\omega_p = 10^{-3}$. The size parameter $q = \omega_p a/c = 1.7$. **b**, Magnetic Fano resonance for a particle with negative μ, $\varepsilon = 1$ and size parameter $q = 0.7$. **c**,**d**, Contour plots of radar back scattering (**c**) and forward scattering (**d**) cross-sections in the vicinity of electric and magnetic quadrupole on the plane $\{\varepsilon, \mu\}$ parameters in the material with negative refractive index. The size parameter (q) is equal to 0.7. The insets shows corresponding three-dimensional plots.

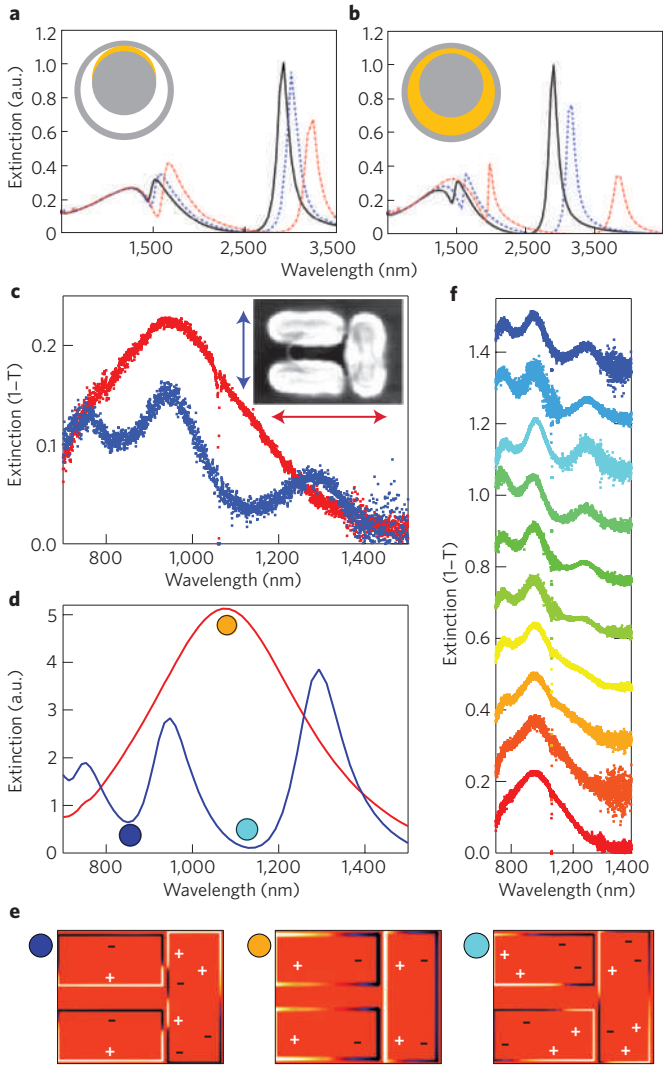

Figure 4 | Extinction spectra of non-concentric ring/disk cavity[22] and a plasmonic dolmen structure[25]. **a**,**b**, Effect on extinction spectrum of partial (**a**) and complete (**b**) filling of the cavity (yellow areas in the inset) with a dielectric medium of permittivity 1 (black solid), 1.5 (blue dashed) and 3 (red dotted). The structure is placed on a glass substrate modelled using a permittivity of 2.04. Note that the wavelength scale is different in the two panels. **c**, Experimentally observed single-dolmen structure extinction spectra for the two polarizations indicated in the inset. **d**, Numerically calculated extinction spectra. **e**, Surface charge distribution for the two Fano resonances in the extinction spectrum for perpendicular polarization and for the extinction peak for parallel polarization. **f**, Measured extinction spectra as the polarization of the incoming light beam is continuously rotated between the two principal directions. Figure reproduced with permission from ref. 22: **a**,**b**, © 2008 ACS; ref. 25: **c**–**f**, © 2009 ACS.

In these types of material, the spectral shape of the Fano resonance will depend sensitively on the specific frequency dependence of $\varepsilon(\omega)$ and $\mu(\omega)$. Metamaterials described using the effective medium approximation have both dipole and quadrupole terms (the electric quadrupole term must be retained in the model provided the magnetic dipole moment is taken into consideration[43]). This means that metamaterials are 'predisposed' to possessing Fano resonances.

Anisotropy can also enhance Fano resonances in optical materials. For a spherical particle with both radial $\{\varepsilon_r, \mu_r\}$ and transverse $\{\varepsilon_t, \mu_t\}$ anisotropies, an exact solution to the scattering problem, similar to Mie theory, can be obtained[69]. The intensity of the surface plasmon resonance can be greatly enhanced in such anisotropic materials. The intensity of the Fano resonance is enhanced with an increasing ratio of $\varepsilon_t/\varepsilon_r > 1$. Similar Fano resonance enhancement can also be obtained for core–shell particles such as nanoshells, owing to the ability to easily tune their dipole and quadrupole resonances[70,71].

Fano resonances in plasmonic nanostructures

Although Fano resonances occur in light scattering from simple spherical particles, the damping of typical metals is too large for the Fano resonance to be clearly observed. The fundamental criterion for a Fano resonance is the interference between a spectrally overlapping broad resonance or continuum and a narrow discrete resonance. These conditions can be satisfied using tunable coupled plasmonic structures made of conventional plasmonic materials such as silver or gold. In contrast to spherical particles, both the widths and the energies of the plasmon resonances are independently controlled by changing the geometry of and spacing between individual structures.

Much of the original work on plasmonic Fano resonances was carried out on metallic arrays. Here the broad resonance providing the continuum for the narrow Fano resonance is a strongly radiative collective dipolar mode formed from a coupling of the plasmons on the individual array elements.

Probably the first theoretical prediction and subsequent experimental realization of Fano resonances in individual plasmonic structures in the optical regime was in dolmen-type slab arrangements[72] and the non-concentric ring/disk cavity[23,24,27]. The structure of this latter system is illustrated in the inset in Fig. 4a. For the concentric ring/disk cavity, the interaction between disk and ring plasmons is diagonal in multipolar symmetry. The interaction between the dipolar disk and ring plasmons results in a hybridized low-energy dipolar bonding resonance and a higher-energy antibonding resonance. The lower-energy bonding resonance is subradiant and very narrow, as the individual dipole moments of the disk and ring are aligned oppositely, reducing the radiative damping. The broad antibonding higher-energy dipolar mode is super-radiant, radiating strongly because the dipolar plasmons of the individual disk and ring are aligned and oscillate in phase. This mode thus provides a broad continuum.

Symmetry breaking in the concentric ring/disk cavity allows coupling between the narrow quadrupolar ring plasmon modes and the antibonding super-radiant dipolar continuum (Fig. 4a, black line). For a system of sufficient size and appropriate ring thickness, the quadrupole mode can be tuned to energies overlapping the continuum, satisfying the conditions for a Fano resonance. A representative spectrum of a non-concentric ring/disk cavity is shown in Fig. 4a (black line). A pronounced quadrupolar Fano resonance appears at the wavelength of 1.5 μm. The experimental realization of such a nanoscopic classical Fano system has recently been demonstrated[27]. An interesting property of the Fano resonance in large non-concentric ring/disk cavity systems is that by simply changing the excitation angle, the incident light can couple directly to the quadrupolar ring mode[22]. This direct coupling will interfere with the 'normal' interference responsible for the Fano resonance and alter its lineshape. As the angle of incidence is changed from perpendicular to grazing, the Fano lineshape is continuously modified from a characteristic asymmetric resonance to a symmetric one. Both the spectral position and the Fano resonance lineshape exhibit a high sensitivity to the dielectric permittivity of the environment (Fig. 4a,b). Higher-order Fano resonances can arise in this system if the dipolar, continuum-like spectrum of the nanoscale resonator is broad enough to overlap with the narrow octupolar resonances. An experimental realization of such a system involving a dolmen-type structure is shown in Fig. 4c–f (ref. 25). The experimental spectra (Fig. 4c,f) were obtained using single-particle confocal extinction spectroscopy, and can be clearly identified with the corresponding constituent modes (Fig. 4d) by means of the calculated charge distributions (Fig. 4e).

Another family of nanostructures that can exhibit sharp Fano resonances is finite clusters (oligomers) of plasmonic nanoparticles. Nanoparticle aggregates exhibit plasmonic modes that are linear combinations of the plasmon modes of each constituent nanoparticle for sufficiently small interparticle separations. For symmetric nano particle clusters, one can classify these collective plasmon modes using group theory. One example of such a structure is the symmetric septamer or heptamer shown in Fig. 5, consisting of a central particle surrounded by six equivalent nanoparticles of the same diameter[24,34]. The point group of this structure is D_{6h} and the collective modes with finite in-plane dipole moments all belong to the E_{1u} irreducible representation. Owing to the specific symmetry of this structure, the collective plasmon modes are hybridized states formed by the interaction of the central particle plasmons with the collective plasmon modes of the surrounding six-particle ring structure as illustrated in Fig. 5a. In this structure, the dipole moment of the collective ring mode and the dipole moment of the central particle are almost equal. The resulting bonding mode consists of individual dipolar nanoparticle plasmons oscillating in phase and along the direction of incident polarization. For finite-size nanoparticles, this mode is super-radiant, that is, it exhibits a strong radiative damping and is broadened into a continuum. However, for the antibonding mode, the dipolar plasmon of the central particle oscillates out of phase with the dipolar mode of the surrounding ring of nanoparticles. The net dipole moment of the antibonding mode is therefore nearly zero, resulting in a subradiant plasmon mode that induces a sharp Fano resonance in the super-radiant continuum as illustrated in Fig. 5b–d. This Fano resonance, which is remarkably insensitive to small structural defects and distortions of the heptamer[24], was recently observed in the scattering spectra of a self-assembled nanoshell heptamer[73] and lithographically fabricated heptamer planar disk clusters[74]. Because the Fano resonance in the heptamer is a consequence of the symmetry of the structure rather than the shape of the individual particles, nanolithography methods offer unique possibilities for tuning its spectral properties by structural and geometric control. Fig. 5d illustrates the effects of nanoparticle coupling on the Fano resonance of the heptamer. Here we see how the coupling between the nanoparticles increases with decreasing interparticle distance, resulting in a strong Fano resonance for the compact heptamer. When removing the central plasmonic dot, the counter-oscillating dipole is absent and the destructive interference that causes the Fano interference is turned off (Fig. 5d, right panel). Figure 5e shows two examples of Fano resonances in a hexamer and an octumer cluster consisting of a central particle and a surrounding ring of particles[75]. For the hexamer of equally sized particles (top left panel), the dipole moment of the ring is smaller than the dipole moment of the central particle. Consequently, the antibonding state possesses a net total dipole moment, is no longer subradiant, and therefore does not induce a sharp Fano resonance. By decreasing the size of the central particle, the antibonding mode becomes subradiant and a clear Fano resonance is induced (top right panel). For the octumer consisting of equal-size particles (bottom left panel), the dipole moment of the ring is larger than for the central particle. By increasing the size of the central particle, the antibonding mode becomes subradiant and induces a sharp Fano resonance (bottom right panel). Figure 5f shows the extraordinary potential of nanoparticle oligomers for localized surface plasmon resonance (LSPR) sensing. As the Fano resonance is very sharp, large and clearly observable shifts of the

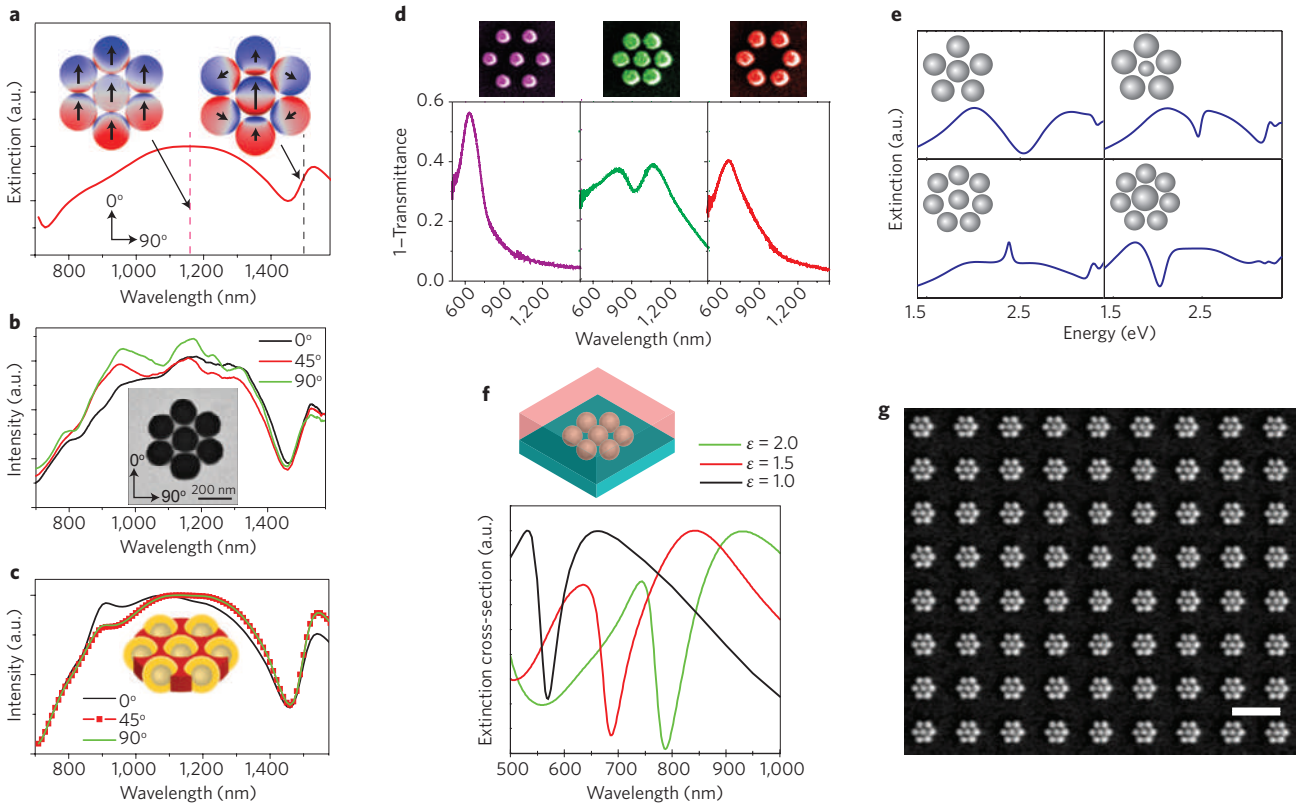

Figure 5 | Fano resonances in plasmonic nanoparticle clusters. a, Calculated dipole amplitudes of the bonding and antibonding collective dipolar plasmon modes in a gold nanoshell heptamer[73]. **b**,**c**, Measured (**b**) and calculated (**c**) scattering spectra of a gold nanoshell heptamer[73]. **d**, Transmission spectra showing the effects of coupling in lithographically fabricated gold nanodisk heptamers[74]. **e**, Extinction spectra showing how the Fano resonance in silver nanosphere hexamers and octumers depend on the size of the central particle[75]. **f**, Effect of a surrounding dielectric medium on the extinction spectrum of a silver nanosphere heptamer. **g**, Example of a large-scale substrate consisting of lithographically fabricated gold nanodisk heptamers[74]. Scale bar: 1 μm. Figure reproduced with permission from ref. 73: **a**–**c**, © 2010 AAAS; ref. 74: **d**,**g**, © 2010 ACS; ref. 75: **e**, © 2010 Springer; ref. 24: **f**, © 2010 ACS.

Fano resonance can be observed when the surrounding dielectric medium of the cluster is changed. The calculated figure of merit for LSPR sensing by this structure is larger than ten (ref. 24). Another significant advantage of lithographically fabricated substrates is that large areas of structures can be fabricated as illustrated[74] in Fig. 5g. Such macroscopic lithographically fabricated substrates hold significant potential in chemical and biological sensing applications as well as for surface-enhanced Raman scattering substrates.

Fano resonances in metallic photonic crystals

In periodic metallic structures, that is, metallic photonic crystals, Fano resonances are abundant. For example, an array of gold nanowires placed on a single-mode slab waveguide exhibits a Fano resonance in extinction in transverse electric (TE) polarization owing to coupling between the array and the waveguide (Fig. 6). The narrow waveguide mode interferes with a continuum of vacuum states. In transverse magnetic (TM) polarization, the incident light can excite a particle plasmon across the gold nanowires, which can interfere destructively with the narrow waveguide resonance. The light in the waveguide interferes destructively with the re-emitted light of the particle plasmon.

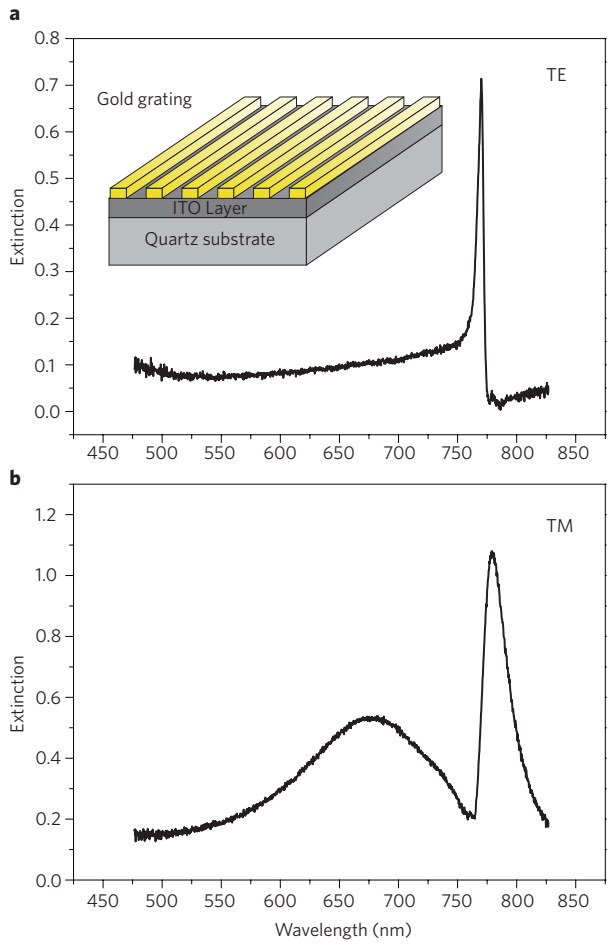

Figure 6 | Fano resonances in a metallic photonic crystal, consisting of a gold nanowire grating on a single-mode indium tin oxide (ITO) slab waveguide, in which the light is incident normal to the structure. **a**, Extinction in TE polarization (*E*-field parallel to the gold wires). A single Fano resonance owing to grating coupling into the waveguide is visible. **b**, Extinction in TM polarization (*E*-field perpendicular to the wires). Two polariton branches that exhibit a Fano lineshape owing to the coupling of the narrow waveguide resonance to the broad particle plasmon in the gold wires are visible.

On changing the incident angle of excitation or the grating period, the spectral dispersion shows pronounced anticrossing behaviour, a signature of waveguide-particle-plasmon polaritons[15,16]. In linear as well as in nonlinear experiments[76], the Fano lineshape can be well described by a two-oscillator model with coupled narrow and broad oscillators[77]. These lineshapes are very stable even under the influence of strong correlated and uncorrelated structural disorder[78].

Fano resonances in metamaterials

Fano resonances in metamaterials were observed for the first time in asymmetrically split-ring arrays (Fig. 7)[30]. When excited by an electromagnetic wave at microwave frequencies, the two uneven arcs of the split-ring structure support in-phase current oscillations (I and III), except in a narrow frequency range in which an antisymmetric current is established. The antisymmetric excitations form an array of magnetic dipoles oscillating perpendicular to the plane of the metamaterial. This collective subradiant mode couples only weakly to free space through interaction with a much broader super-radiant dipole mode of in-phase currents, creating a classical Fano complex. The transmission band is accompanied by a steep normal dispersion, enabling low group velocities, electromagnetically induced transparency (EIT)-like and slow-light behaviour in both passive and gain-assisted metamaterials[57]. Polarization-sensitive Fano resonances linked to strong optical activity and circular dichroism in the microwave and optical parts of the spectrum can be engaged through constructing a chiral arrangement of the metamaterial array with respect to the incident electromagnetic wave[79]. A Fano metamaterial with polarization-insensitive resonances, with behaviour independent of incidence direction of light, has also been introduced[80]. Fano resonances have recently been observed in a superconducting metamaterial, promising extremely high-Q modes[81].

A dramatic collapse of Fano resonance has been observed in metamaterials where the appearance of high-Q modes resulted from correlated (coherent) excitations of metamolecules in the ensemble[82]. The discovery of Fano resonances in coherent metamaterials has led to the concept of the 'lasing spaser', which combines metamaterial and spaser ideas to create a narrow-divergence, coherent source of electromagnetic radiation. The lasing spaser is fuelled by collective, gain-assisted dark plasmonic oscillations that leak into free space through a highly radiating mode in a classical Fano arrangement[83].

Plasmon-induced transparency in metamaterials

Under certain conditions a Fano resonance can be regarded as the classical analogue of electromagnetically induced transparency[30,57,72]. These conditions are: (i) sufficiently small frequency detuning between the two coupled resonances; (ii) strongly contrasting resonance linewidths; and (iii) appropriate resonance amplitudes. When coherent coupling between the two resonances occurs, destructive interference can suppress the absorption of the broader resonance, resulting in an induced transparency window. In metamaterials, nearly full transparency can be achieved[30]; and the residual absorption is only due to losses arising from Drude damping in the metal. Radiative losses can be nearly completely suppressed[28,49].

One structure that allows the experimental observation of plasmon-induced transparency is a two-layer metallic metamaterial consisting of a single-wire dipole antenna coupled to a two-wire quadrupole antenna. This is based on an idea[72] that the near-field coupling of a spectrally broad dipole resonance with a narrow quadrupole resonance in a dolmen-type structure can lead to plasmon-induced transparency, as the limiting case of the Fano coupling shown in Fig. 4. Nevertheless, lateral coupling suffers from difficulties in nanofabrication, requiring accurate reproducibility of the very small gaps between nanostructures. Vertical stacking of the metamaterial elements can circumvent this stringent requirement.

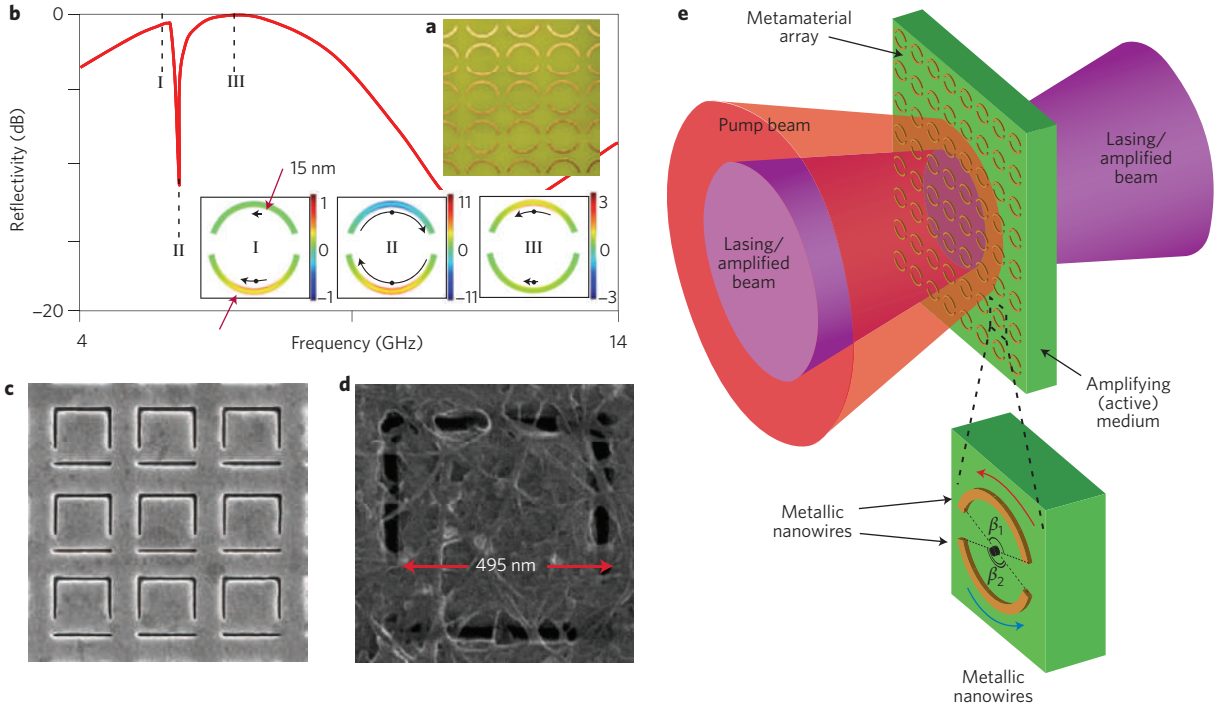

Figure 7 | Fano resonances in metamaterials. a,**b**, In a microwave metamaterial — an array of wire asymmetric split rings (**a**) — Fano reflection resonance (**b**) is formed by the interference of the high-*Q* magnetic dipole mode of excitation (II) and low-*Q* electric dipole modes (I and III)[30]. Black arrows indicate instantaneous directions of the current flow. **c**, A photonic Fano metamaterial, in the form of an array of asymmetric slits in a gold film manufactured by focused ion beam. This structure is complementary to **a** and is simplified for nanofabrication. **d**, A unit cell of such a photonic metamaterial functionalized with a 'nanoscale feature' of single-walled carbon nanotubes and imaged with a helium-ion microscope shows enhanced ultrafast nonlinear response owing to plasmon–exciton coupling[89]. **e**, Conceptual design of the lasing spaser[83], a lasing device fuelled by plasmonic oscillations at the Fano resonance. Figure reproduced with permission from ref. 30: **a**,**b**, © 2007 APS; ref. 89: **c**,**d**, © 2010 APS; ref. 83: **e**, © 2008 NPG.

In such a multilayer geometry (see Fig. 8), homogeneous spacer distances of 20–30 nm are easily achievable during a normal stacking process. The resulting metamaterial structure (Fig. 8a) also uses structural symmetry breaking to enhance the coupling of the dipole mode to the quadrupole mode in the adjacent underlying layer. A displacement of a few tens of nanometres is sufficient to realize good coupling efficiency, and prominent induced transparency, which agrees very well with an EIT-type Fano model (Fig. 8b).

Applications

As Fano resonances arise from the interference between two or more oscillators, they possess an inherent sensitivity to changes in geometry or local environment: small perturbations can induce dramatic resonance or lineshape shifts. This property renders Fano-resonant media particularly attractive for a range of applications, some recently demonstrated, but many not yet foreseen.

Perhaps the most straightforward application of Fano resonant media is in the development of chemical or biological sensors. Here, the introduction of a layer of molecules in the immediate environment of a Fano-resonant structure can induce an unexpectedly large spectral shift in the resonance frequency, as indicated for the non-concentric disk/ring cavity of Fig. 4. Detection limits that approach single-molecule binding events may be possible. This effect, in combination with the appropriate biomarkers, could enable a new generation of label-free chemical and bioanalysis probes adaptable to high-throughput applications[49]. Efficient LSPR sensing has been demonstrated in asymmetric split-ring resonators[84,85], and in a dolmen-type structure, where the EIT Fano resonance shows a sensitivity to the presence of glucose in aqueous solution[49]. In the latter case, the active sensing geometry of an asymmetric 'H' structure, with its localized light modes probing attolitre or zeptolitre volumes around each sensing element, is simple and mass-producible. This geometry possesses very high LSPR sensitivities of nominally 600 nm per refractive-index unit and figures of merit in the range of 5. In another example, a Fano metamaterial shows extraordinary sensitivity to the presence of a single atomic layer of graphene on its surface[86]. The optical transmission increases multifold at the resonance frequency, which is linked to a Fano-type plasmonic mode supported by the periodic metallic nanostructure. These experiments were performed with chemical-vapour-deposited graphene covering a number of size-scaled metamaterial samples with plasmonic modes at different frequencies ranging from 1,600 to 1,800 nm.

A similar sensitivity to local displacement or deformation of Fano-resonant structures, perturbing their coupled oscillator characteristics, can also be exploited for sensing of physical parameters such as displacement, temperature or pressure. This can be accomplished by fabrication of Fano-resonant media on flexible or deformable substrates. The deformation of the substrate would perturb the resonance and result in a simple, electronics-free sensor with a straightforward optical readout.

The integration of Fano-resonant structures with nonlinear and phase-change media[87–89] provides many opportunities for applications in switching and electro-optics. Asymmetric split-ring structures have been used in frequency tunable near-infrared metamaterials based on the VO_2 phase transition[87] and in a nanoscale-thickness electro-optical modulator based on the phase change transition in chalcogenide glass[88]. A carbon nanotube composite metamaterial with strong coupling between weakly radiating Fano-type resonant plasmonic modes and excitonic responses of single-walled semiconductor carbon nanotubes was recently demonstrated. It shows an exceptionally strong ultrafast near-infrared optical nonlinearity emerging through the exciton–plasmon interaction[89].

We predict that electro-optic control of the angular light-scattering properties of Fano-resonant structures could lead to new

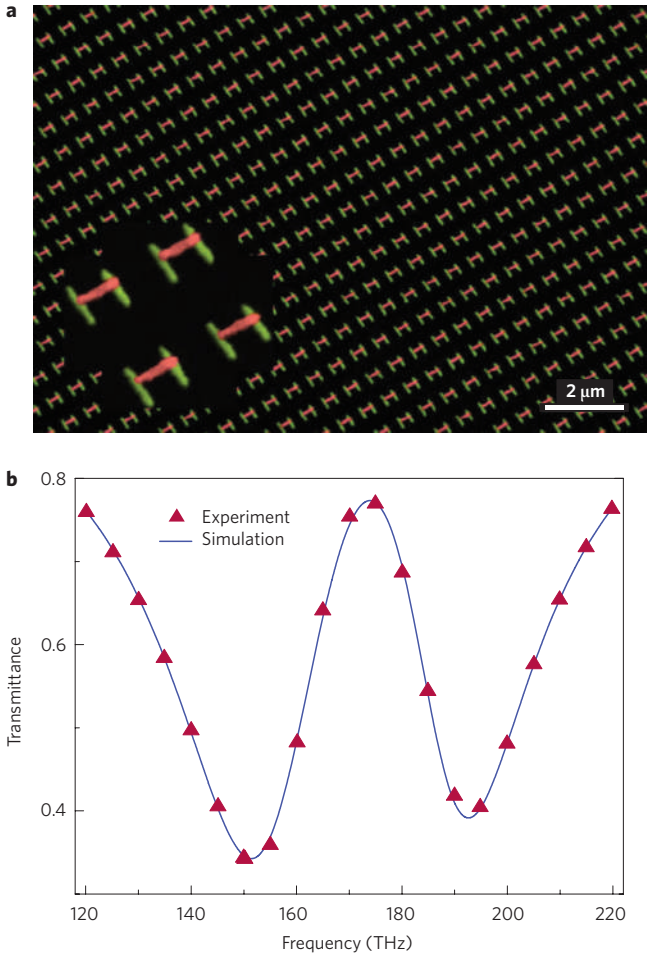

Figure 8 | EIT in metamaterials. a, Scanning electron microscope image of the stacked plasmonic EIT analogue structure. The red colour represents the gold bar in the top layer and the green colour represents the gold wire pair in the bottom layer. Inset: enlarged view. **b**, Experimental transmittance spectrum of the sample. The fitting curve was calculated from a Fano-type EIT model simulation. Figure reproduced with permission from ref. 28: **a**, © 2009 NPG.

electronic displays of various sizes, even compact projectors. This control could be facilitated by Fano-resonant structures composed of mixed plasmonic and excitonic media, such as semiconductor carbon nanotubes[89] or quantum dots[83], with metallic plasmon-resonant nanostructures. Fano-resonant media in a waveguide geometry[90] could provide a method for decreasing the radiative losses and thereby increase the propagation lengths[91,92], and also provide active switching strategies.

Future outlook

Although Fano resonances in plasmonic materials and metamaterials have been realized only recently, we can already see many promising strategies for further enhancement of this behaviour. In addition, the unique properties associated with this lineshape are highly promising for potential applications. Future integration of this effect into new optical media can transition this fascinating physical property into a wide range of technologies. The design of Fano resonances into optical systems may give rise to new nonlinear and switchable metamaterials, ultrasensitive media for chemical or biosensing, and new types of optical switches, interferometers, nanoantennas, displays, and other devices. Fano-resonant media could find useful applications in near-field imaging, high-quality optical waveguides, and contrast enhancement in imaging. The challenge now exists to translate this unique resonant behaviour into large-area materials and active devices.

References

1. Rabinovitch, M. I. & Trubetskov, D. I. *Oscillations and Waves in Linear and Nonlinear Systems* (Kluwer Academic Publishers, 1989).
2. Fano, U. Effects of configuration interaction on intensities and phase shifts. *Phys. Rev.* **124,** 1866–1878 (1961).
3. Miroshnichenko, A. E., Flach, S. & Kivshar, Y. S. Fano resonances in nanoscale structures. Preprint at http://arxiv.org/abs/0902.3014 (2009).
4. Luo, H. G., Xiang, T., Wang, X. Q., Su, Z. B. & Yu, L. Fano resonance for Anderson impurity systems. *Phys. Rev. Lett.* **92,** 256602 (2004).
5. Johnson, A. C., Marcus, C. M., Hanson, M. P. & Gossard, A. C. Coulomb-modified Fano resonance in a one-lead quantum dot. *Phys. Rev. Lett.* **93,** 106803 (2004).
6. Kobayashi, K., Aikawa, H., Sano, A., Katsumoto, S. & Iye, Y. Fano resonance in a quantum wire with a side-coupled quantum dot. *Phys. Rev. B* **70,** 035319 (2004).
7. Hessel, A. & Oliner, A. A. A new theory of Wood's anomalies on optical gratings. *Appl. Opt.* **4,** 1275–1297 (1965).
8. Sarrazin, M., Vigneron, J. P. & Vigoureux, J. M. Role of Wood anomalies in optical properties of thin metallic films with a bidimensional array of subwavelength holes. *Phys. Rev. B* **67,** 085415 (2003).
9. Lee, H-T. & Poon, A. W. Fano resonances in prism-coupled square micropillars. *Opt. Lett.* **29,** 5–7 (2004).
10. Rybin, M. V. *et al.* Fano resonance between Mie and Bragg scattering in photonic crystals. *Phys. Rev. Lett.* **103,** 023901 (2009).
11. Fan, S. H. Sharp asymmetric line shapes in side-coupled waveguide-cavity systems. *Appl. Phys. Lett.* **80,** 908–910 (2002).
12. Fan, S. H. & Joannopoulos, J. D. Analysis of guided resonances in photonic crystal slabs. *Phys. Rev. B* **65,** 235112 (2002).
13. Genet, C., van Exter, M. P. & Woerdman, J. P. Fano-type interpretation of red shifts and red tails in hole array transmission spectra. *Opt. Commun.* **225,** 331–336 (2003).
14. Fan, S. H., Suh, W. & Joannopoulos, J. D. Temporal coupled-mode theory for the Fano resonance in optical resonators. *J. Opt. Soc. Am. A* **20,** 569–572 (2003).
15. Christ, A., Tikhodeev, S. G., Gippius, N. A., Kuhl, J. & Giessen, H. Waveguide-plasmon polaritons: Strong coupling of photonic and electronic resonances in a metallic photonic crystal slab. *Phys. Rev. Lett.* **91,** 183901 (2003).
16. Christ, A. *et al.* Optical properties of planar metallic photonic crystal structures: Experiment and theory. *Phys. Rev. B* **70,** 125113 (2004).
17. Sarrazin, M. & Vigneron, J-P. Bounded modes to the rescue of optical transmission. *Europhys. News* **38,** 27–31 (2007).
18. Catrysse, P. B. & Fan, S. H. Near-complete transmission through subwavelength hole arrays in phonon-polaritonic thin films. *Phys. Rev. B* **75,** 075422 (2007).
19. Ruan, Z. & Fan, S. Temporal coupled-mode theory for Fano resonance in light scattering by a single obstacle. *J. Phys. Chem. C* **114,** 7324–7329 (2009).
20. Tribelsky, M. I., Flach, S., Miroshnichenko, A. E., Gorbach, A. V. & Kivshar, Y. S. Light scattering by a finite obstacle and Fano resonances. *Phys. Rev. Lett.* **100,** 043903 (2008).
21. Miroshnichenko, A. E. *et al.* Fano resonances: A discovery that was not made 100 years ago. *Opt. Phot. News* **19,** 48 (2008).
22. Hao, F. *et al.* Symmetry breaking in plasmonic nanocavities: Subradiant LSPR sensing and a tunable Fano resonance. *Nano Lett.* **8,** 3983–3988 (2008).
23. Hao, F., Nordlander, P., Sonnefraud, Y., Van Dorpe, P. & Maier, S. A. Tunability of subradiant dipolar and Fano-type plasmon resonances in metallic ring/disk cavities: Implications for nanoscale optical sensing. *ACS Nano* **3,** 643–652 (2009).
24. Mirin, N. A., Bao, K. & Nordlander, P. Fano resonances in plasmonic nanoparticle aggregates. *J. Phys. Chem. A* **113,** 4028–4034 (2009).
25. Verellen, N. *et al.* Fano resonances in individual coherent plasmonic nanocavities. *Nano Lett.* **9,** 1663–1667 (2009).
26. Maier, S. A. The benefits of darkness. *Nature Mater.* **8,** 699–700 (2009).
27. Sonnefraud, Y. *et al.* Experimental realization of subradiant, superradiant, and Fano resonances in ring/disk plasmonic nanocavities. *ACS Nano* **4,** 1664–1670 (2010).
28. Liu, N. *et al.* Plasmonic analogue of electromagnetically induced transparency at the Drude damping limit. *Nature Mater.* **8,** 758–762 (2009).
29. Shvets, G. & Urzhumov, Y. A. Engineering the electromagnetic properties of periodic nanostructures using electrostatic resonances. *Phys. Rev. Lett.* **93,** 243902 (2004).
30. Fedotov, V. A., Rose, M., Prosvirnin, S. L., Papasimakis, N. & Zheludev, N. I. Sharp trapped-mode resonances in planar metamaterials with a broken structural symmetry. *Phys. Rev. Lett.* **99,** 147401 (2007).
31. Christ, A. *et al.* Controlling the Fano interference in a plasmonic lattice. *Phys. Rev. B* **76,** 201405 (2007).
32. Auguié, B. & Barnes, W. L. Collective resonances in gold nanoparticle arrays. *Phys. Rev. Lett.* **101,** 143902 (2008).
33. Bachelier, G. *et al.* Fano profiles induced by near-field coupling in heterogeneous dimers of gold and silver nanoparticles. *Phys. Rev. Lett.* **101,** 197401 (2008).
34. Le, F. *et al.* Metallic nanoparticle arrays: A common substrate for both surface-enhanced Raman scattering and surface-enhanced infrared absorption. *ACS Nano* **2,** 707–718 (2008).

35. Yan, J-Y., Zhang, W., Duan, S., Zhao, X-G. & Govorov, A. O. Optical properties of coupled metal-semiconductor and metal-molecule nanocrystal complexes: Role of multipole effects. *Phys. Rev. B* **77,** 165301 (2008).
36. Kivshar, Y. S. Nonlinear optics: The next decade. *Opt. Express* **16,** 22126–22128 (2008).
37. Ekinci, Y. *et al.* Electric and magnetic resonances in arrays of coupled gold nanoparticle in-tandem pairs. *Opt. Express* **16,** 13287–13295 (2008).
38. Neubrech, F. *et al.* Resonant plasmonic and vibrational coupling in a tailored nanoantenna for infrared detection. *Phys. Rev. Lett.* **101,** 157403 (2008).
39. Nygaard, N., Piil, R. & Mølmer, K. Feshbach molecules in a one-dimensional optical lattice. *Phys. Rev. A* **77,** 021601 (2008).
40. Pistolesi, F., Blanter, Y. M. & Martin, I. Self-consistent theory of molecular switching. *Phys. Rev. B* **78,** 085127 (2008).
41. Cho, D. J., Wang, F., Zhang, X. & Shen, Y. R. Contribution of the electric quadrupole resonance in optical metamaterials. *Phys. Rev. B* **78,** 121101 (2008).
42. Christ, A., Martin, O. J. F., Ekinci, Y., Gippius, N. A. & Tikhodeev, S. G. Symmetry breaking in a plasmonic metamaterial at optical wavelength. *Nano Lett.* **8,** 2171–2175 (2008).
43. Petschulat, J. *et al.* Multipole approach to metamaterials. *Phys. Rev. A* **78,** 043811 (2008).
44. Naether, U., Rivas, D. E., Larenas, M. A., Molina, M. I. & Vicencio, R. A. Fano resonances in waveguide arrays with saturable nonlinearity. *Opt. Lett.* **34,** 2721–2723 (2009).
45. Chen, C-Y., Un, I-W., Tai, N-H. & Yen, T-J. Asymmetric coupling between subradiant and superradiant plasmonic resonances and its enhanced sensing performance. *Opt. Express* **17,** 15372–15380 (2009).
46. Cubukcu, E., Zhang, S., Park, Y. S., Bartal, G. & Zhang, X. Split ring resonator sensors for infrared detection of single molecular monolayers. *Appl. Phys. Lett.* **95,** 043113 (2009).
47. Kanté, B., de Lustrac, A. & Lourtioz, J. M. In-plane coupling and field enhancement in infrared metamaterial surfaces. *Phys. Rev. B* **80,** 035108 (2009).
48. Miroshnichenko, A. E. *et al.* Dynamics and instability of nonlinear Fano resonances in photonic crystals. *Phys. Rev. A* **79,** 013809 (2009).
49. Liu, N. *et al.* Planar metamaterial analogue of electromagnetically induced transparency for plasmonic sensing. *Nano Lett.* **10,** 1103–1107 (2010).
50. Miroshnichenko, A. E. Non-rayleigh limit of the lorenz-Mie solution and suppression of scattering by spheres of negative refractive index. *Phys. Rev. A* **80,** 013808 (2009).
51. Miroshnichenko, A. E. Instabilities and quasi-localized states in nonlinear Fano-like systems. *Phys. Lett. A* **373,** 3586–3590 (2009).
52. Miroshnichenko, A. E. Nonlinear Fano-Feshbach resonances. *Phys. Rev. E* **79,** 026611 (2009).
53. Pakizeh, T., Langhammer, C., Zoric, I., Apell, P. & Käll, M. Intrinsic Fano interference of localized plasmons in Pd nanoparticles. *Nano Lett.* **9,** 882–886 (2009).
54. Pakizeh, T. & Käll, M. Unidirectional ultracompact optical nanoantennas. *Nano Lett.* **9,** 2343–2349 (2009).
55. Parsons, J. *et al.* Localized surface-plasmon resonances in periodic nondiffracting metallic nanoparticle and nanohole arrays. *Phys. Rev. B* **79,** 073412 (2009).
56. Li, Z-P., Shegai, T., Haran, G. & Xu, H-X. Multiple-particle nanoantennas for enormous enhancement and polarization control of light emission. *ACS Nano* **3,** 637–642 (2009).
57. Papasimakis, N. & Zheludev, N. I. Metamaterial-induced transparency: Sharp Fano resonances and slow light. *Opt. Phot. News* **20,** 22–27 (2009).
58. Urzhumov, Y. A., Korobkin, D., Neuner, B., Zorman, C. & Shvets, G. Optical properties of sub-wavelength hole arrays in SiC membranes. *J. Opt. A* **9,** S322–S333 (2007).
59. Ebbesen, T. W., Lezec, H. J., Ghaemi, H. F., Thio, T. & Wolff, P. A. Extraordinary optical transmission through sub-wavelength hole arrays. *Nature* **391,** 667–669 (1998).
60. Garcia-Vidal, F. J., Martin-Moreno, L., Ebbesen, T. W. & Kuipers, L. Light passing through subwavelength apertures. *Rev. Mod. Phys.* **82,** 729–787 (2010).
61. Stockman, M. I., Faleev, S. V. & Bergman, D. J. Localization versus delocalization of surface plasmons in nanosystems: Can one state have both characteristics? *Phys. Rev. Lett.* **87,** 167401 (2001).
62. Born, M. & Wolf, E. *Principles of Optics* 7th edn (Cambridge Univ. Press, 1999).
63. Bohren, C. F. & Huffman, D. R. *Absorption and Scattering of Light by Small Particles* (Wiley, 1998).
64. Tribelsky, M. I. & Luk'yanchuk, B. S. Anomalous light scattering by small particles. *Phys. Rev. Lett.* **97,** 263902 (2006).
65. Luk'yanchuk, B. S. *et al.* Peculiarities of light scattering by nanoparticles and nanowires near plasmon resonance frequencies in weakly dissipating materials. *J. Opt. A* **9,** S294–S300 (2007).
66. Bystrov, A. M. & Gildenburg, V. B. Dipole resonances of an ionized cluster. *J. Exp. Theor. Phys.* **100,** 428–439 (2005).
67. Wang, Z. B., Luk'yanchuk, B. S., Hong, M. H., Lin, Y. & Chong, T. C. Energy flow around a small particle investigated by classical Mie theory. *Phys. Rev. B* **70,** 035418 (2004).
68. Luk'yanchuk, B. S. *et al.* Extraordinary scattering diagram for nanoparticles near plasmon resonance frequencies. *Appl. Phys. A* **89,** 259–264 (2007).
69. Luk'yanchuk, B. S. & Qiu, C-W. Enhanced scattering efficiencies in spherical particles with weakly dissipating anisotropic materials. *Appl. Phys. A* **92,** 773–776 (2008).
70. Brown, L. V., Sobhani, H., Lassiter, J. B., Nordlander, P. & Halas, N. J. Heterodimers: Plasmonic properties of mismatched nanoparticle pairs. *ACS Nano* **4,** 819–832 (2010).
71. Hu, Y., Noelck, S. J. & Drezek, R. A. Symmetry breaking in gold-silica-gold multilayer nanoshells. *ACS Nano* **4,** 1521–1528 (2010).
72. Zhang, S., Genov, D. A., Wang, Y., Liu, M. & Zhang, X. Plasmon-induced transparency in metamaterials. *Phys. Rev. Lett.* **101,** 047401 (2008).
73. Fan, J. A. *et al.* Self-assembled plasmonic nanoparticle clusters. *Science* **328,** 1135–1138 (2010).
74. Hentschel, M. *et al.* Transition from isolated to collective modes in plasmonic oligomers. *Nano Lett.* **10,** 2721–2726 (2010).
75. Bao, K., Mirin, N. & Nordlander, P. Fano resonances in planar silver nanosphere clusters. *Appl. Phys. A* **100,** 333–339 (2010).
76. Zentgraf, T., Christ, A., Kuhl, J. & Giessen, H. Tailoring the ultrafast dephasing of quasiparticles in metallic photonic crystals. *Phys. Rev. Lett.* **93,** 243901 (2004).
77. Klein, M. W., Tritschler, T., Wegener, M. & Linden, S. Lineshape of harmonic generation by metallic nanoparticles and metallic photonic crystal slabs. *Phys. Rev. B* **72,** 115113 (2005).
78. Nau, D. *et al.* Correlation effects in disordered metallic photonic crystal slabs. *Phys. Rev. Lett.* **98,** 133902 (2007).
79. Plum, E. *et al.* Metamaterials: Optical activity without chirality. *Phys. Rev. Lett.* **102,** 113902 (2009).
80. Papasimakis, N. *et al.* Metamaterial with polarization and direction insensitive resonant transmission response mimicking electromagnetically induced transparency. *Appl. Phys. Lett.* **94,** 211902 (2009).
81. Fedotov, V. A. *et al.* Temperature control of Fano resonances and transmission in superconducting metamaterials. *Opt. Express* **18,** 9015–9019 (2010).
82. Fedotov, V. A. *et al.* Spectral collapse in ensembles of meta-molecules. *Phys. Rev. Lett.* **104,** 223901 (2010).
83. Zheludev, N. I., Prosvirnin, S. L., Papasimakis, N. & Fedotov, V. A. Lasing spaser. *Nature Photon.* **2,** 351–354 (2008).
84. Debus, C. & Bolivar, P. H. Terahertz biosensors based on double split ring arrays. *Proc. SPIE* **6987,** 6987OU (2008).
85. Lahiri, B., Khokhar, A. Z., De La Rue, R. M., McMeekin, S. G. & Johnson, N. P. Asymmetric split ring resonators for optical sensing of organic materials. *Opt. Express* **17,** 1107–1115 (2009).
86. Papasimakis, N. *et al.* Graphene in a photonic metamaterial. *Opt. Express* **18,** 8353–8359 (2010).
87. Dicken, M. J. *et al.* Frequency tunable near-infrared metamaterials based on VO_2 phase transition. *Opt. Express* **17,** 18330–18339 (2009).
88. Sámson, Z. L. *et al.* Metamaterial electro-optic switch of nanoscale thickness. *Appl. Phys. Lett.* **96,** 143105 (2010).
89. Nikolaenko, A. E. *et al.* Carbon nanotubes in a photonic metamaterial. *Phys. Rev. Lett.* **104,** 153902 (2010).
90. Maier, S. A. *et al.* Local detection of electromagnetic energy transport below the diffraction limit in metal nanoparticle plasmon waveguides. *Nature Mater.* **2,** 229–232 (2003).
91. Kawata, S., Ono, A. & Verma, P. Subwavelength colour imaging with a metallic nanolens. *Nature Photon.* **2,** 438–442 (2008).
92. Liu, M., Lee, T-W., Gray, S. K., Guyot-Sionnest, P. & Pelton, M. Excitation of dark plasmons in metal nanoparticles by a localized emitter. *Phys. Rev. Lett.* **102,** 107401 (2009).

Acknowledgements

The authors acknowledge valuable technical assistance from Dr Nikolay A. Mirin, J. Britt Lassiter and Shaunak Mukherjee. The research presented in this paper is supported in part by the Agency for Science, Technology and Research (A*STAR) for financial support (THz S&T Inter-RI Program, Project 082 141 0039, SERC Metamaterials Program on Superlens, grant no. 092 154 0099 and A*STAR TSRP Program, grant no. 102 152 0018) (B.L. and C.T.C.); the UK Engineering and Physical Sciences Research Council and the Royal Society (S.A.M. and N.I.Z.); the US Department of Defense NSSEFF (N.J.H.), the Robert A. Welch Foundation C-1220 and C-1222, and the Center for Advanced Solar Photophysics, a Energy Frontier Research Center funded by the US Department of Energy (N.J.H. and P.N.); and the Deutsche Forschungsgemeinschaft of the Federal Republic of Germany (FOR 557, FOR 730, SPP1391) and the Bundesministerium für Bildung und Forschung (H.G.) for support.

Author contributions

B.L. and C.T.C. initiated the section 'The Fano resonance'. N.I.Z. initiated the section 'Fano resonances in metamaterials'. S.A.M., N.J.H. and P.N. initiated the section 'Fano resonances in plasmonic nanostructures'. H.G. initiated the sections 'Fano resonances in metallic photonic crystals' and 'Plasmon-induced transparency in metamaterials'. All authors contributed equally to the 'Applications' section and to editing. B.L., P.N. and N.J.H. carried out the main final edits.

Additional information

The authors declare no competing financial interests.